

Research Article

Adaptive Modulation and Coding Control Based on Human Body Channel Characteristics Under Different WBAN Scenarios

Dairoku Muramatsu* 

Department of Mechanical and Intelligent Systems Engineering, Graduate School of Informatics and Engineering, The University of Electro-Communications, Tokyo, Japan

Abstract

Wireless Body Area Network (WBAN) enables continuous health monitoring by interconnecting wearable and implantable sensors, but their links suffer from strongly scenario-dependent human-body propagation effects that conventional physical-layer (PHY) designs do not address. Most prior studies assess limited WBAN links, so a unified strategy that spans all scenarios remains missing. This work presents a comprehensive adaptation framework across all three IEEE 802.15.6ma communication scenarios with minimal feedback overhead, ensuring consistent performance under diverse channel conditions. This study aims to maximize WBAN throughput by adaptively selecting the modulation and coding scheme according to channel characteristics unique to three IEEE 802.15.6ma communication scenarios: 21 MHz on-body, 400 MHz in-body, and 2.4 GHz off-body. By leveraging finite-difference time-domain analysis on a detailed whole-body voxel model combined with a compact hybrid antenna, we capture realistic, wideband channel responses that reflect both on-skin and implanted device environments. Wide-band channel responses were first obtained with finite-difference time-domain analysis of the whole-body voxel model combined with a compact hybrid antenna that integrates galvanic electrodes and patch radiators. The channel responses were fed into link-level simulations covering BPSK, QPSK, GMSK and 16-QAM, with and without BCH (63, 51) coding. QPSK was most efficient at mid-range SNR, whereas coded 16-QAM became superior once E_b/N_0 exceeded roughly 10 dB, boosting off-body throughput by up to 35%. Applying simple E_b/N_0 thresholds (≈ 6 -13 dB) to switch between QPSK and coded 16-QAM almost doubled the data rate versus a fixed conservative scheme while still meeting the error-free requirement of medical telemetry. These results highlight the practical benefits of our adaptive control approach for real-world WBAN deployments, including reduced power consumption and simplified transceiver design.

Keywords

Wearable/Implantable Sensor, Healthcare, Wireless Body Area Network, Physical Layer, Human Body Communication, Narrowband Wireless Communication, Radio Propagation Channel Characteristics, Antenna, Human Body Effect, Electromagnetic Field Analysis, Modulation and Coding, Modulation and Coding

*Corresponding author: dmuramatsu@uec.ac.jp (Dairoku Muramatsu)

Received: 6 May 2025; Accepted: 20 May 2025; Published: 20 June 2025



Copyright: © The Author(s), 2025. Published by Science Publishing Group. This is an **Open Access** article, distributed under the terms of the Creative Commons Attribution 4.0 License (<http://creativecommons.org/licenses/by/4.0/>), which permits unrestricted use, distribution and reproduction in any medium, provided the original work is properly cited.

1. Introduction

Against the backdrop of population ageing, lifestyle-related diseases, and recent pandemics, preventive medicine—encompassing primary prevention to avert disease onset and secondary prevention to detect illnesses early and initiate prompt treatment—has become indispensable. At the same time, reducing the costs and human resources required to maintain health is an urgent issue. In this context, wearable and implantable devices equipped with diverse biosensing functions have emerged through advances in integration technology. By continuously measuring, collecting, and monitoring a user's health status, such wearable/implantable healthcare systems (Figure 1) are expected to prevent serious diseases [1-3].

A multitude of wearable/implantable devices and sensors worn by the user are interconnected via on-body communication over the skin surface [4] and in-body communication between the inside and the outside of the body [5]. Furthermore, a hub device connects to an external terminal located away from the user via off-body communication, transmitting the acquired biological signals to medical servers in real time for health monitoring.

As the wireless networking technology surrounding the user that supports such healthcare systems, the wireless body area network (WBAN) has been standardized in IEEE 802.15.6ma [6-9]. Designed mainly for medical and healthcare applications, the standard defines several different physical layers (PHY) (Table 1). In general, the radio propagation channel in wireless communication exhibits characteristics that differ from conventional wireless channels due to the presence of the human body [10, 11]. Moreover, WBAN specifies three distinct communication scenarios—on-body, in-body, and off-body—whose channel characteristics differ markedly, making the selection of an appropriate communication scheme for each scenario essential. However, most studies on WBAN communication schemes concentrate on a limited scenario [12-16]. In contrast to the scenario-specific frameworks and control schemes in [12-16], our method uses unified thresholds tailored to each of the three WBAN scenarios. The threshold-based switching relies solely on locally measured link quality, eliminating the need for continuous control signaling and reducing implementation complexity. Future WBAN applications are also envisioned in fitness [17], entertainment [18], and user interface domains [19], where even higher data rates may be required.

This study demonstrates that high-throughput WBAN communication can be achieved by adaptively controlling the modulation and coding schemes based on human-body channel characteristics obtained via numerical electromagnetic analysis under different WBAN scenarios. Chapter 2 describes the electromagnetic analysis setup for calculating the body-channel characteristics and presents the results for each scenario. Chapter 3 outlines the communication-system simulation configured with those characteristics and clarifies the throughput performance for the assumed combinations of modulation and coding. Chapter 4 concludes the paper.

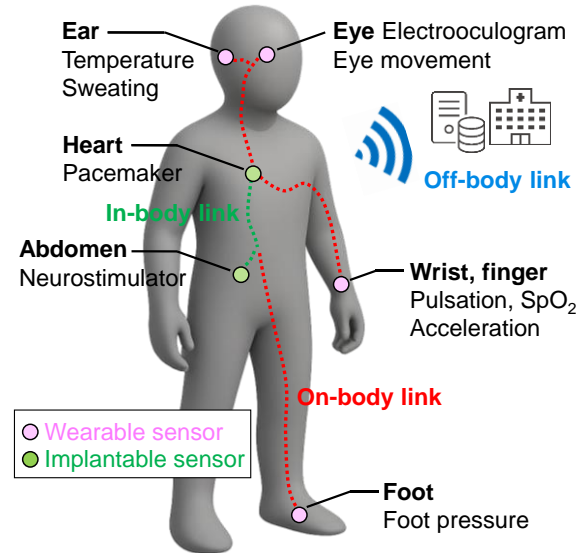


Figure 1. Wearable/Implantable healthcare and WBAN.

Table 1. WBAN Communication scenarios and physical layers.

Scenario	On-body communication	In-body communication	Off-body communication
Target	Wearable device	Implantable device	External device
Usage	Inter-sensor collaboration	Exchange medical control information	Data transmission to access point
PHY	Human body communication (21 MHz), Narrowband wireless communication (400, 920 MHz, 2.4 GHz) Ultra wide band communication (3.1-10.6 GHz)		

2. Channel Characteristics Calculation

The human-body channel model in this work is calculated by numerical electromagnetic analysis incorporating human body and antenna models. Section 2.1 introduces the numerical human model, Section 2.2 the antenna model, Section 2.3 the three assumed WBAN scenarios and the corresponding analysis setup, and Section 2.4 the channel characteristics obtained.

2.1. Numerical Human Body Model

The body-channel model is calculated using the finite-difference time-domain (FDTD) method. As a numerical whole-body human model with detailed anatomical structures, we employ TARO, provided by the National Institute of Information and Communications Technology [20] (Figure 2 shows its exterior and internal structure rendered by volume visualization). TARO was originally developed to evaluate human exposure to electromagnetic waves radiated from the electronic devices such as mobile phones (e.g., currents induced in tissue and heat stress due to energy absorption).

The model represents an average Japanese adult male (height = 173.2 cm, weight = 65 kg) and consists of ~8 million cubic voxels, each with an edge length of 2 mm, to which the electrical properties of the corresponding tissue or organ are assigned. To accurately evaluate the wide-band interaction between the body and antennas in WBAN channels, a Debye-dispersion frequency-dependent model is applied to the electrical properties of every voxel [21].

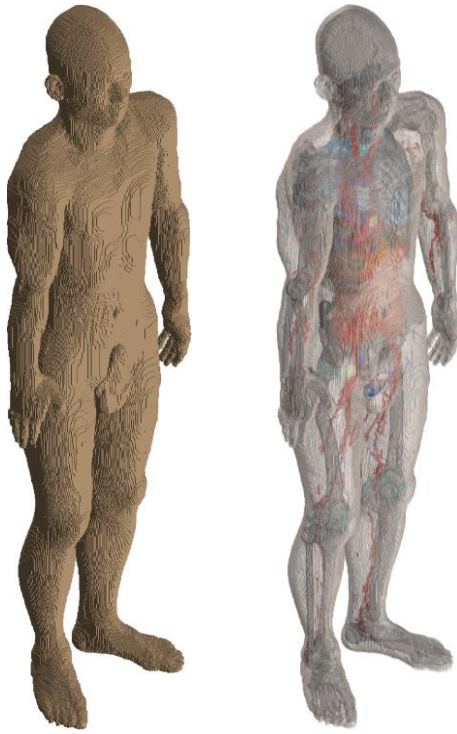


Figure 2. Whole-body numerical human model TARO [20].

2.2. Antenna Structure

A WBAN requires that the user wear or implant communication antennas. This study applies a compact antenna [22] to a wearable and implantable WBAN. The antenna fuses two distinct structures: electrodes that operate at 21 MHz for on-body links and radiating patch that operate at 400 MHz for in-body links and 2.4 GHz for off-body links. Figure 3 shows the antenna's detailed geometry. The ground electrode of the human body communication electrodes is shared with the ground plate of a patch antenna, reducing antenna volume to a size suitable for compact wearable or implantable devices [23]. In addition, exciting three different frequency bands from a single feed point enables further miniaturization and a substantial reduction in RF components.

All electrodes, radiating elements, and feed wires in the numerical antenna model are modeled as perfect conductors. A lossless dielectric with a relative permittivity of 1.3 is loaded between the electrodes and patch to adjust the resonance frequency and bandwidth. Dimensions of the radiators and micro-strip feed line are fine-tuned to the target bands. The finalized values are $h = 4$ mm, $L_d = 24$ mm, $W_d = 24$ mm, $L_p = 13$ mm, $W_p = 18$ mm, $W_m = 1$ mm, $L_g = 8$ mm, $W_g = 0.5$ mm, $W_e = 24$ mm, $L_e = 8$ mm. As shown in the reflection-coefficient characteristics (Figure 4), the antenna resonates at 400 MHz and 2.4 GHz, and the electrode part functions as the signal-transmission element for human body communication at 21 MHz [24, 25].

When deploying this antenna in an implantable environment, it must not only deliver improved performance but also be robust against the influence of the electrical properties of surrounding biological tissues [26]. Additionally, considering the size constraints of small implantable devices, further miniaturization using parasitic elements and similar techniques is also a critical challenge [27].

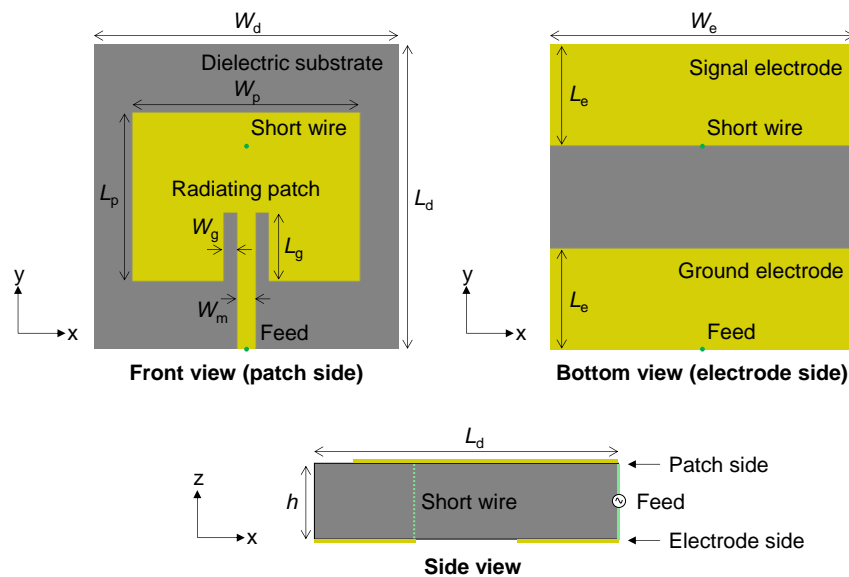


Figure 3. Structure of compact antenna for wearable/implantable communication.

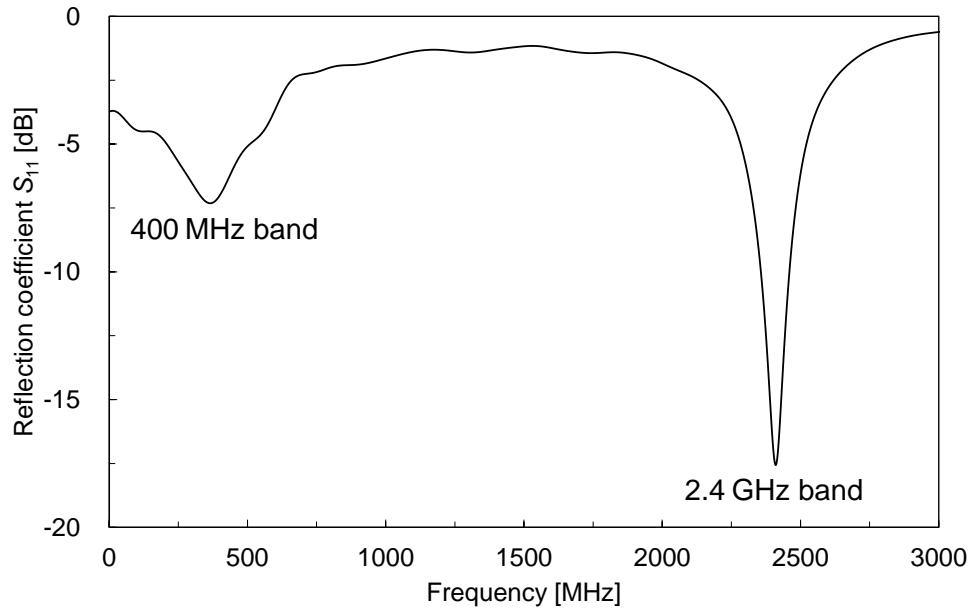


Figure 4. Reflection characteristics of wearable/implantable antenna as a function of frequency.

2.3. Electromagnetic Field Analysis Setup

Three WBAN scenarios are assumed (Figure. 5):

- 1) On-body: communication between a hub device on the lower abdomen and a wearable device on the chest (e.g., an ECG sensor).
- 2) In-body: communication between the hub and an implantable device in the lower abdomen (e.g., a neurostimulator).
- 3) Off-body: communication between the hub and an external device 1 m away (e.g., a wireless access point).

The whole-body model TARO (Section 2.1) is used for the analysis. The hub terminal on the lower-abdominal surface (#1), the wearable device on the chest surface (#2), and the implantable device inside the lower abdomen (#3) all use the wearable/implantable antenna described in Section 2.2. The external device (#4), located 1 m from the hub terminal, is equipped with a dipole antenna resonant in the 2.4 GHz band.

Electromagnetic field analysis is carried out with XFDTD (Remcom Inc., PA, USA) based on the FDTD method. The free-space distance from the model edge to the absorbing boundary is set to about 20 cells. A non-uniform mesh is used, with the minimum cell size of 0.2 mm around the antennas, gradually coarsening to a maximum of 2 mm. A 7-layer perfectly matched layer is employed for the absorbing boundary. The source is a band-limited wideband pulse optimized for each scenario. Time steps are 0.597 ps (on-body) and 0.614 ps (in-body and off-body).

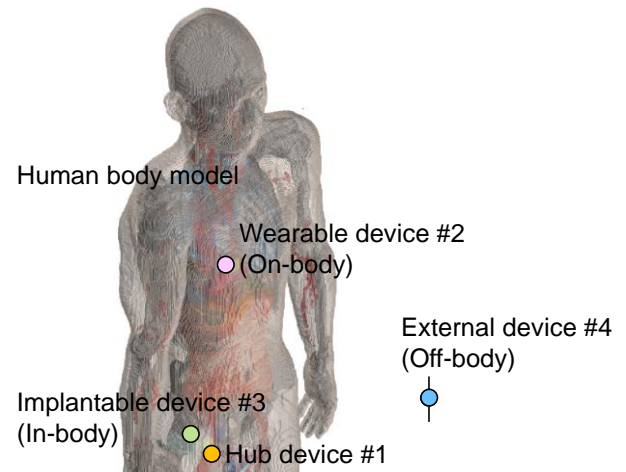


Figure 5. Antenna placement inside and outside the human model.

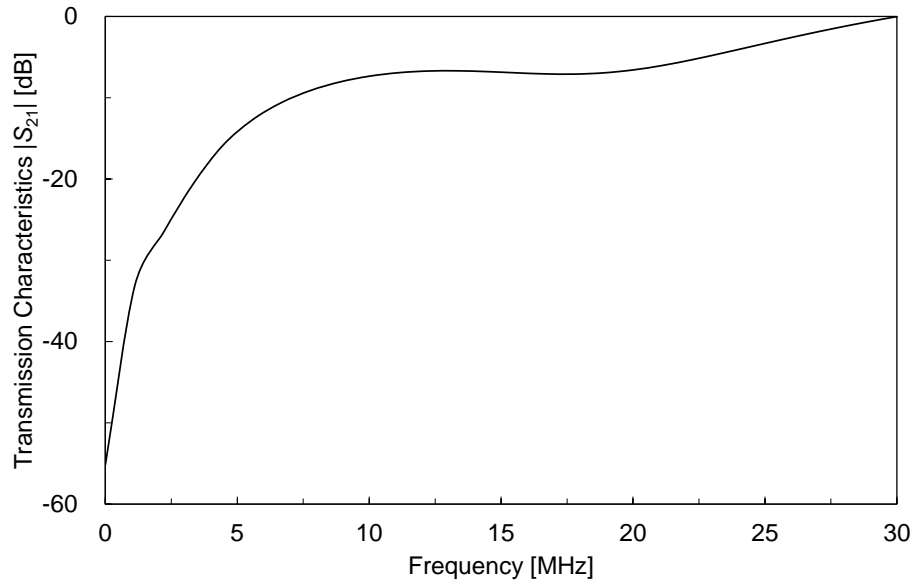
2.4. Channel Characteristics Under Each WBAN Scenario

Figure 6(a)-(c) show the frequency response $|S_{n1}|$ of the human body channel measured under each scenario. The subscript in $|S_{n1}|$ corresponds to #1-#4 in Figure 5, and each trace is normalized to the maximum value within its respective scenario. The characteristics differ widely owing to factors such as device placement, frequency band, and the frequency-dependent electrical properties of tissues interacting with the antennas. This indicates that each scenario requires an optimal modulation, coding, and control scheme. Chapter 3 employs these characteristics in communication-system simulations, referencing the IEEE 802.15.6ma PHY, to investigate optimal control.

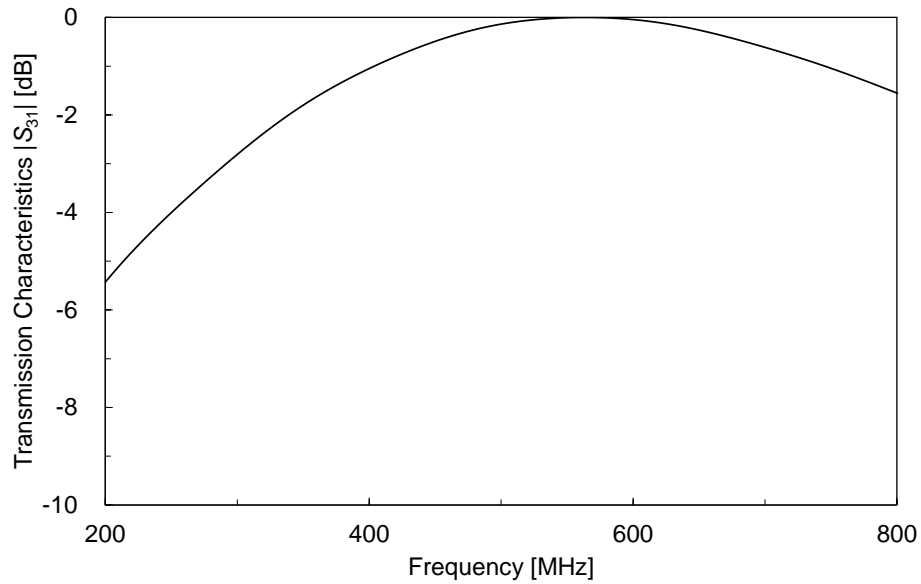
3. Communication Scheme Analysis Based on Channel Characteristics

The communication performance is evaluated by computer simulation incorporating the body-channel characteristics into

the transmission path. Section 3.1 describes the simulation setup, and Section 3.2 presents throughput characteristics for different modulation-coding combinations under the three WBAN scenarios and discusses adaptive control.



(a) 21 MHz On-body



(b) 400 MHz In-body

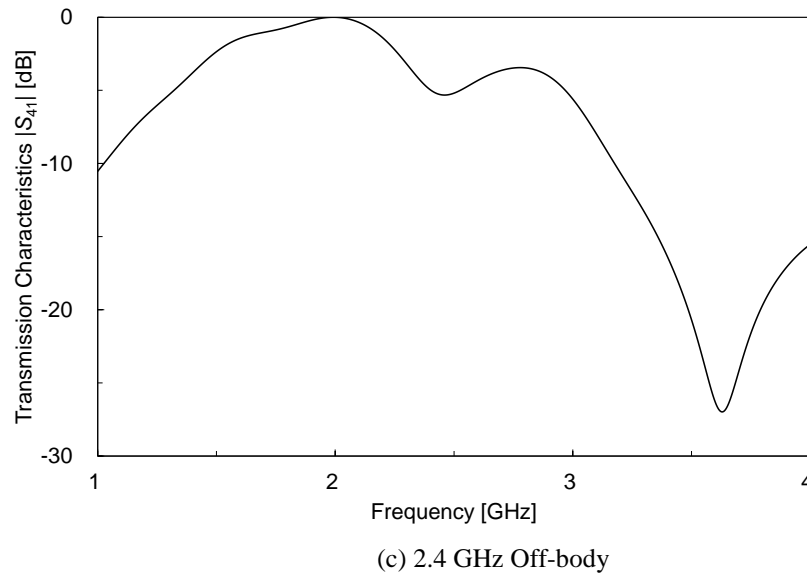


Figure 6. Channel characteristics under WBAN scenarios.

3.1. Simulation Parameters

Using the channel characteristics from Chapter 2, we simulate three IEEE 802.15.6ma scenarios: on-body at 21 MHz, in-body at 400 MHz, and off-body at 2.4 GHz. The simulations use MATLAB Simulink with time-domain Monte Carlo methods. A random 100,000-bit data stream is encoded, modulated, transmitted through the body channel with additive white Gaussian noise, demodulated and decoded, and the bit-error rate is computed to derive the error-free throughput.

Table 2 lists the parameters of the simulation. Bands follow the IEEE recommendations: 18.37-23.62 MHz (on-body), 402-403 MHz (in-body), and 2.4-2.48 GHz (off-body). Four modulation schemes are considered: BPSK, QPSK, GMSK, and 16-QAM (constellations in Figure 7). Higher-order modulations increase data rate per time and bandwidth but are more error-prone under poor channel environments. BPSK, QPSK, and GMSK are adopted in IEEE 802.15.6ma; 16-QAM is additionally examined. Symbol rates follow the occupied bands, with root-raised-cosine or Gaussian filtering for band-limiting. Although 64-QAM can theoretically offer higher throughput at favorable channel conditions, it requires highly linear RF front ends with high-resolution A/D con-

verters—demands beyond the power and hardware constraints of typical WBAN nodes. Moreover, the narrow noise margin of 64-QAM makes it extremely vulnerable to minor channel fluctuations, risking unacceptable bit-error rates. Therefore, we limit our highest-order modulation to 16-QAM to balance throughput, robustness, and low-power implementation.

Channel coding employs the BCH (63, 51) code used in the standard, with code rate 0.81 (51 information bits + 12 parity bits). We selected BCH (63, 51) because, compared to Low-Density Parity-Check (LDPC) and turbo codes, it enables non-iterative algebraic decoding with significantly lower computational complexity and energy consumption. Additionally, relative to convolutional codes offering similar error-correction capability, BCH (63, 51) requires fewer parity bits, thereby preserving throughput and simplifying hardware implementation. Moreover, as the coding scheme specified in the IEEE 802.15.6 standard, BCH (63, 51) ensures compliance and interoperability with existing WBAN devices. Lower code rates reduce throughput but improve robustness, especially for higher-order modulation. Two cases—without coding and with BCH coding—are compared. Thus, for the three scenarios, four modulations, and two coding options, throughput versus E_b/N_0 is obtained.

Table 2. Parameters of communication scheme simulation.

Scenario	On-body communication	In-body communication	Off-body communication
PHY	21 MHz Human body communication	400 MHz Narrowband wireless comm.	2.4 GHz Narrowband wireless comm.
Band	18.37-23.62 MHz	402-405 MHz	2.4-2.48 GHz
Modulation	BPSK, QPSK, GMSK, 16-QAM		
Coding	BCH (63, 51): an error-correcting code with a total length of 63 bits, comprising 51 data bits and 12 parity bits		

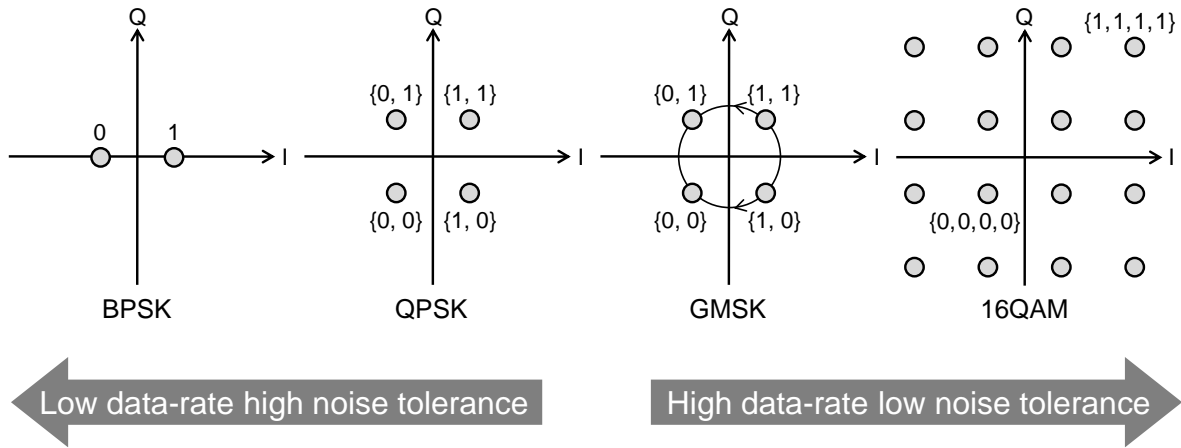


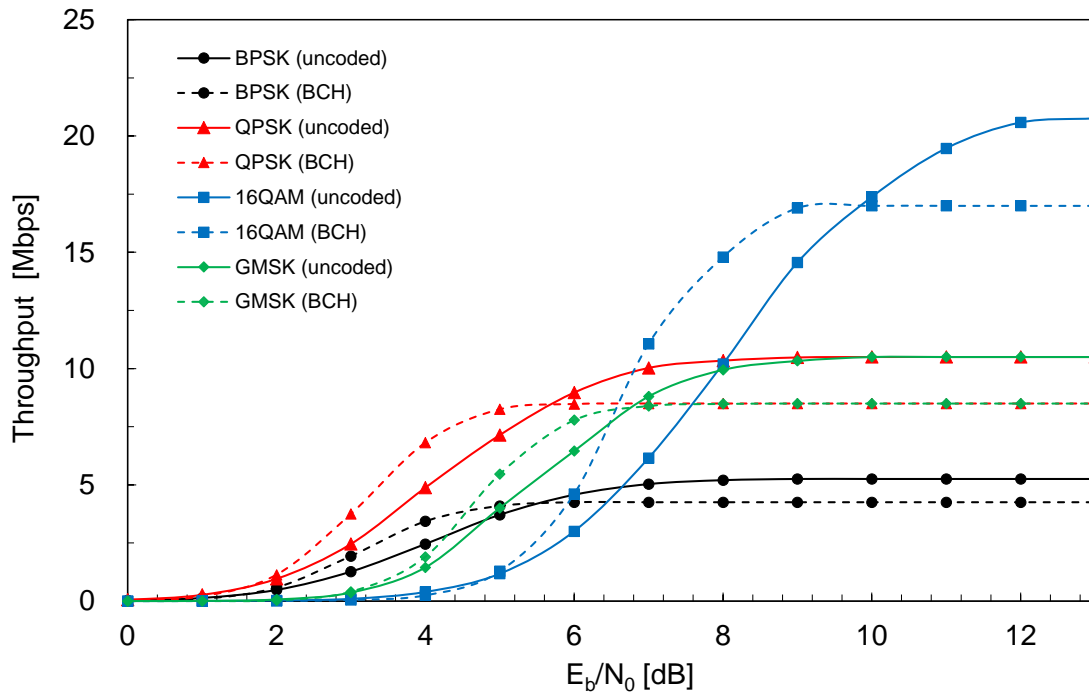
Figure 7. Constellation diagrams of each modulation scheme.

3.2. Evaluation of Modulation-coding Schemes

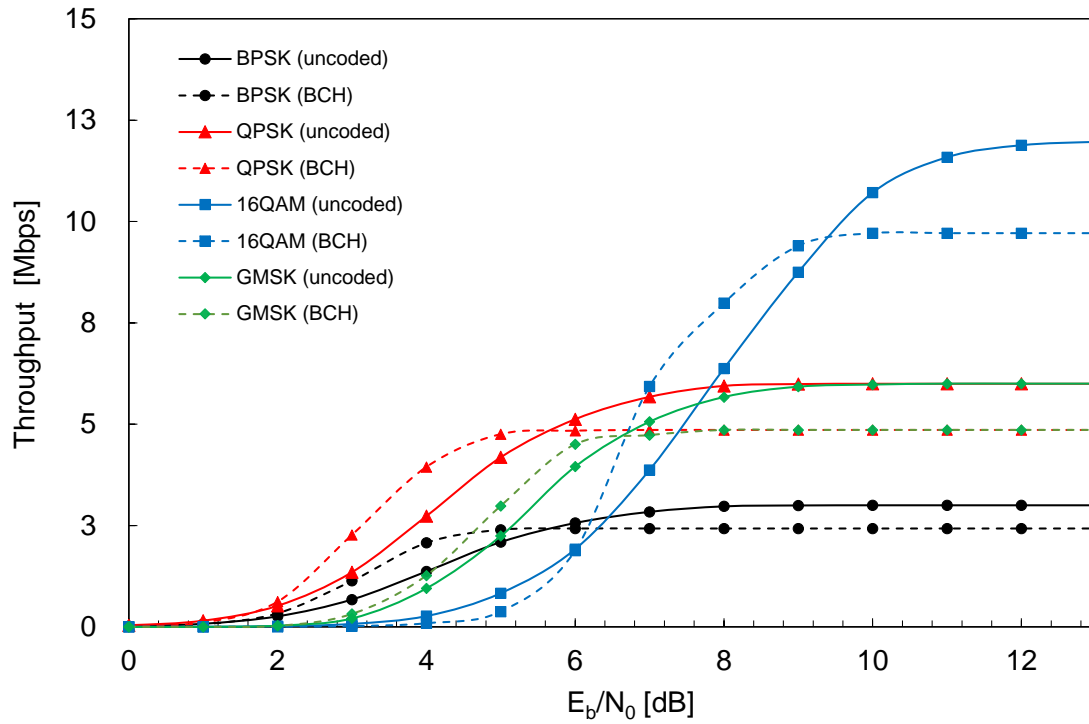
Throughput curves versus E_b/N_0 are shown in Figure 8(a)-(c). In all scenarios the best performance is given by QPSK and 16-QAM owing to relatively flat in-band channel responses. However, the optimal E_b/N_0 thresholds for switching modulation differ: 5.5, 7, 10 dB (on-body); 5.5, 7, 9.5 dB (in-body); and 6, 8, 13 dB (off-body).

Figure 8(c) also shows that for off-body communication, coding markedly improves throughput with 16-QAM, because the wider band intensifies inter-symbol interference and degrades noise tolerance, which the coding mitigates.

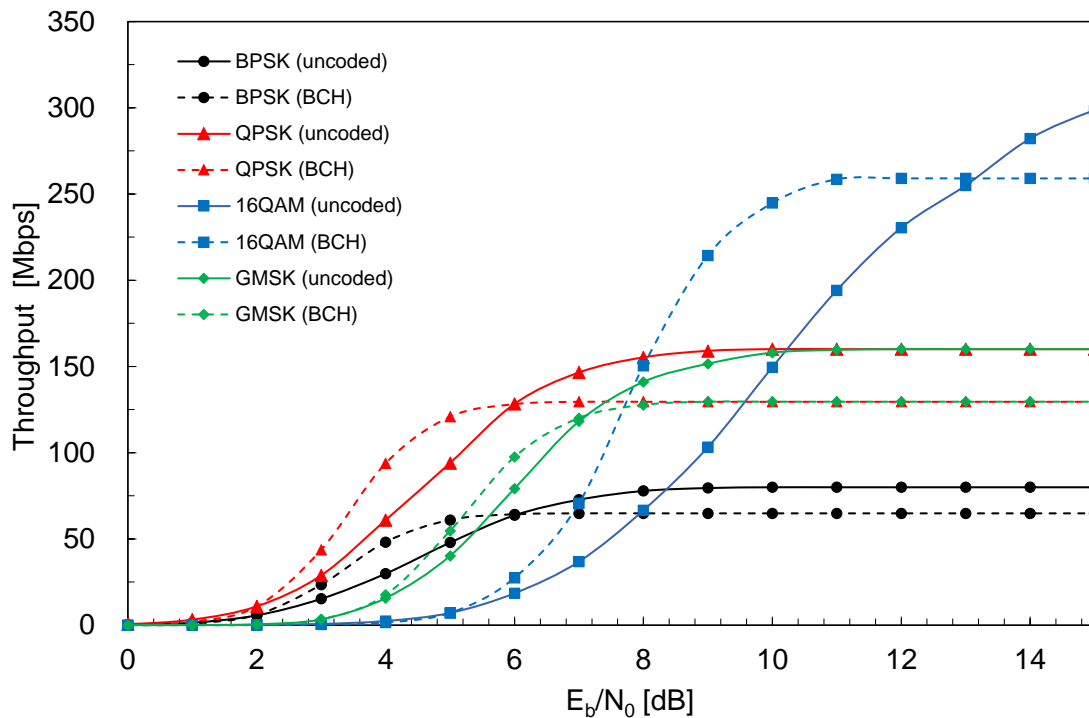
These results reveal that each WBAN scenario—21 MHz on-body, 400 MHz in-body, and 2.4 GHz off-body—has its own optimal modulation-coding scheme and adaptive control strategy.



(a) 21 MHz On-body



(b) 400 MHz In-body



(c) 2.4 GHz Off-body

Figure 8. Throughput characteristics as a function of E_b/N_0 .

4. Conclusions

Using a numerical human model and wearable/implantable

antenna model, we calculated radio-propagation channel characteristics inside and around the body. Communication scheme simulations then compared combinations of modulation and coding to maximize throughput under multiple

WBAN scenarios, clarifying the optimal scheme for each. These findings define the conditions for high-performance communication under varying channel states. Stable, high-speed links among sensors on and in the body will enable new healthcare applications such as real-time intrabody video and large-volume multi-channel biological signal transfer. High data-rate realization is also critical for prospective entertainment uses of WBANs. Future work will analyze dynamic channel variations due to body motion and physiological activity and develop more advanced control schemes for real environments. In particular, we will investigate methods to maintain link stability under channel variations induced by walking and gestures, and evaluate how our adaptive thresholds perform under such variability.

Abbreviations

WBAN	Wireless Body Area Network
PHY	Physical Layer
FDTD	Finite-difference Time-domain
ECG	Electrocardiogram
BPSK	Binary Phase-Shift Keying
QPSK	Quadrature Phase-Shift Keying
GMSK	Gaussian Minimum Shift Keying
QAM	Quadrature Amplitude Modulation
BCH	Bose-Chaudhuri-Hocquenghem
LDPC	Low-Density Parity-Check
E_b/N_0	Energy per Bit to Noise Power Spectral Density Ratio

Acknowledgments

I acknowledge the assistance of Mr. K. Nishida in the communication-scheme analysis.

Author Contributions

Dairoku Muramatsu is the sole author. The author read and approved the final manuscript.

Funding

A part of this research was funded by G-7 Scholarship Foundation, JGC-S Scholarship Foundation, Murata Science and Education Foundation, The Foundation for Technology Promotion of Electronic Circuit Board.

Data Availability Statement

The data supporting the outcome of this research work has been reported in this manuscript.

Conflicts of Interest

The author declares no conflicts of interest.

References

- [1] Van Laerhoven, K.; Lo, B.; Ng, J.; Thiemjarus, S.; King, R.; Kwan, S.; Gellersen, H.; Sloman, M.; Wells, O.; Needham, P.; Peters, N.; Darzi, A.; Toumazou, C.; Yang, G.-Z. Medical Healthcare Monitoring with Wearable and Implantable Sensors. Proc. 2nd Int. Workshop on Ubiquitous Computing for Pervasive Healthcare Applications, Nottingham, UK, 2004, pp. 1-4.
- [2] Majumder, S.; Mondal, T.; Deen, M. J. Wearable Sensors for Remote Health Monitoring. *Sensors* 2017, 17(1), 130. <https://doi.org/10.3390/s17010130>
- [3] Vijayan, V.; Connolly, J. P.; Condell, J.; McKelvey, N.; Gardiner, P. Review of Wearable Devices and Data Collection Considerations for Connected Health. *Sensors* 2021, 21(16), 5393. <https://doi.org/10.3390/s21165393>
- [4] Alomainy, A.; Hao, Y.; Hu, X.; Parini, C. G.; Hall, P. S. UWB On-Body Radio Propagation and System Modelling for Wireless Body-Centric Networks. *IEE Proc. Comm.* 2006, 153(1), 107-114. <https://doi.org/10.1049/ip-com:20050046>
- [5] Kiourt, A.; Nikita, K. S. A Review of Implantable Patch Antennas for Biomedical Telemetry: Challenges and Solutions. *IEEE Antennas Propag. Mag.* 2012, 54(3), 210-228. <https://doi.org/10.1109/MAP.2012.6293992>
- [6] IEEE 802.15 Working Group. IEEE 802.15.6ma Technical Requirements Document, IEEE 802.15-21-0577-02-006a, 2021, pp. 1-13. <https://www.ieee802.org/15/pub/TG6ma.html>
- [7] IEEE Computer Society. IEEE Standard for Local and Metropolitan Area Networks, Part 15.6: Wireless Body Area Networks. IEEE, New York, 2012. <https://doi.org/10.1109/IEEESTD.2012.6161600>
- [8] Preethichandra, D. M. G.; Piyathilaka, L.; Izhar, U.; Samarasinghe, R.; De Silva, L. C. Wireless Body Area Networks and Their Applications—A Review. *IEEE Access* 2023, 11, 9202-9220. <https://doi.org/10.1109/ACCESS.2023.3239008>
- [9] Hamdi, A.; Nahali, A.; Harrabi, M.; Brahem, R. Optimized Design and Performance Analysis of Wearable Antenna Sensors for WBAN Applications. *J. Information and Telecommunication* 2023, 7(2), 155-175. <https://doi.org/10.1080/24751839.2023.2179909>
- [10] Hu, Z. H.; Nechayev, Y. I.; Hall, P. S.; Constantinou, C. C.; Hao, Y. Measurements and Statistical Analysis of On-Body Channel Fading at 2.45 GHz. *IEEE Antennas and Wireless Propagation Letters*. 2007, 6, 612-615. <https://doi.org/10.1109/LAWP.2007.904633>
- [11] Movassaghi, S.; Abolhasan, M.; Lipman, J.; Smith, D.; Jamalipour, A. Wireless Body Area Networks: A Survey. *IEEE Communications Surveys & Tutorials*. 2014, 16(3), 1658-1686. <https://doi.org/10.1109/SURV.2013.121313.00064>

- [12] Kang, T., Lim, I., Hwang, J., Hyoun, C., Park, H., Kang, S. A Method of Increasing Data Rate for Human Body Communication System for Body Area Network Applications. In Proceedings of the 2012 IEEE Vehicular Technology Conference (VTC Fall); 2012; pp. 1-5.
<https://doi.org/10.1109/VTCFall.2012.6398980>
- [13] Kobayashi, T., Sugimoto, C., Kohno, R. Performance Evaluation of the Spread Spectrum Human Body Communication Devices. In Proceedings of the 8th International Symposium on Medical Information and Communication Technology (IS-MICT); 2014; pp. 1-4.
<https://doi.org/10.1109/ISMICT.2014.6825207>
- [14] Lin, K.-H., Chen, F.-C. Implementation of Iterative Error Detection and Correction for BAN Transceiver Systems. *Wireless Networks*. 2023, 29(4), 1771-1786.
<https://doi.org/10.1007/s11276-022-03222-3>
- [15] Ito, K. Performance Evaluation and Improvement of PER and Throughput in Galvanic-Coupling Intra-Body Communication Systems. In Proceedings of the 40th Annual International Conference of the IEEE Engineering in Medicine and Biology Society (EMBC); 2018; pp. 3742-3745.
<https://doi.org/10.1109/EMBC.2018.8513354>
- [16] Anzai, D., Koya, T., Wang, J. Throughput Evaluation on Multilevel Modulation with Local Frequency Offset Spatial Diversity for 400 MHz Band Implant Communications. *IET Microwaves, Antennas & Propagation*. 2017, 11(5), 593-599.
<https://doi.org/10.1049/iet-map.2016.0604>
- [17] Sipal, V.; Gaetano, D.; McEvoy, P.; Ammann, M. J. Impact of Hub Location on WBAN Performance for Fitness Applications. *IEEE Antennas Wireless Propag. Lett.* 2015, 14, 1522-1525.
<https://doi.org/10.1109/LAWP.2014.2376943>
- [18] Liao, Y.; Yu, Q.; Zhai, X.; Ai, Q.; Liu, Q.; Zhou, T. Wireless Big Data Meets WBANs: Cooperative Task Processing with MEC. *Proc. IEEE ICC Workshops 2019, Shanghai, China*, pp. 1-5. <https://doi.org/10.1109/ICCW.2019.8756938>
- [19] Maity, S.; Yang, D.; Redford, S. S.; Das, D.; Chatterjee, B.; Sen, S. BodyWire-HCI: New Interaction Modalities via Electro-Quasistatic HBC. *ACM Trans. Comput.-Hum. Interact.* 2020, 27(6), 1-25. <https://doi.org/10.1145/3406238>
- [20] Nagaoka, T.; Watanabe, S.; Sakurai, K.; Kunieda, E.; Watanabe, S. Development of High-Resolution Whole-Body Voxel Models of Average Japanese Adults and RF Dosimetry Applications. *Phys. Med. Biol.* 2004, 49(1), 1-15.
<https://doi.org/10.1088/0031-9155/49/1/002>
- [21] Gabriel, S.; Lau, R. W.; Gabriel, C. The Dielectric Properties of Biological Tissues: II. 10 Hz-20 GHz. *Phys. Med. Biol.* 1996, 41(11), 2251-2269.
<https://doi.org/10.1088/0031-9155/41/11/002>
- [22] Sasaki, Y.; Muramatsu, D. 21 MHz/2.4 GHz Dual-Use Wearable Antenna for IEEE 802.15.6 WBAN. *Proc. IEEE GCCE 2023, Kyoto, Japan, 2023*, pp. 51-52.
<https://doi.org/10.1109/GCCE59613.2023.10315501>
- [23] Sasaki, Y.; Muramatsu, D. Dual-Use Patch Antenna with Defected Ground Plane for Wearable Healthcare Communication. *Proc. Int. Conf. BioSensors, BioElectronics, BioMedical Devices, BioMEMS/NEMS & Applications (Bio4Apps 2023)*, Gold Coast, Australia, Dec. 2023, p. 18.
- [24] Muramatsu, D.; Koshiji, F.; Koshiji, K.; Sasaki, K. Analytical and Experimental Studies on Human Body Communication between Wristwatch and Handheld Device at 10 MHz. *Sensors and Materials* 2014, 26(8), 581-589.
<https://doi.org/10.18494/SAM.2014.1035>
- [25] Nishida, Y.; Sasaki, K.; Yamamoto, K.; Muramatsu, D.; Koshiji, F. Equivalent Circuit Model Viewed from Receiver Side in Human Body Communication. *IEEE Trans. Biomed. Circuits Syst.* 2019, 13(4), 746-755.
<https://doi.org/10.1109/TBCAS.2019.2918323>
- [26] Muramatsu, D.; Sasaki, Y. 2.4 GHz/5.6 GHz Dual-use Wearable Patch Antenna Integrated with Electrodes and Parasitic Element for Wireless Body Area Network. *IEEJ Trans. Electr. Electron. Eng.* 2024, 19(1), 1-3.
<https://doi.org/10.1002/tce.23929>
- [27] Kodama, M.; Muramatsu, D. Determining Carrier Frequency for Implantable Human Body Communication Based on Transmission Efficiency-Electromagnetic Interference Trade-off. *AIP Advances* 2024, 14(7), 1-6.
<https://doi.org/10.1063/5.0210654>